TEMPORAL WAVESHAPING OF A TRIODE COLD CATHODE ELECTRON BEAM GUN

Gary Loda
Beta Development Corporation, 6557 Sierra Lane
Dublin, CA 94566

Sol Schneider*
Little Silver, NJ 07739

William F. Otto and George J. Dezenberg
US Army Missile Command, ATTN: DRSMI-RHS
Redstone Arsenal, AL 35898

Introduction

It was first shown by Loda[1] that the effect of plasma closure on the impedance of cold cathode diode electron beam guns[2] could be greatly reduced by adding a self-biased grid to the gun. Large triode cold cathod electron beam guns are being used by Los Alamos National Laboratory in the ANTARES system.[3] A characteristic of the triode cold cathode e-gun is that a large initial current overshoot occurs as the self-biased grid charges to the operating voltage and the acceleration voltage has a poor rise time when a pulse forming network is used for excitation. Since foil heating is inversely related to e-gun voltage, the voltage rise and fall times should be minimized to reduce the heating. Leland and Kirchner recognized the need for improving the initial triode e-gun transient and suggested using auxiliary circuitry for rapid readjustment of the grid potential after cathode ignition, using a "spark" cathode or reducing the grid-anode capacitance.[4] In this paper the characteristics of a 15 cm by 200 cm beam area "spark" cathode, triode electron beam gun are presented and the modeling and experiments performed to improve its voltage rise time are described.

Experimental

E-Gun

The cross section of the electron beam gun investigated in this work is shown in Figure 1. A perforated stainless steel cathode structure, configured in a Pierce profile, was used to facilitate investigation of different wide area emitters. In this work a "spark" cathode was used with the emitters being 48 separate resistively ballasted surface flashover cathode discs. The discs were arranged in a single row with a 4.1 cm disc separation. The concentric grid was made of solid sixteen guage stainless steel and fitted with an 80% open area molybdenum screen. A field shaping ring was affixed to the grid to improve e-beam uniformity. The separation between the cathode and grid planes as well as between the grid and anode planes was 15 cm. A copper hibatchi structure with 57% open area, sealed with a 1-mil Ti foil, was used as anode.

Modulator

The electron beam gun is driven by the line type modular shown in Figure 2. Three parallel networks were used to facilitate PFN impedance changes for different modes of e-gun operation. Ten stages were used per network with a capacitance value of 0.06 μFd/stage. The stage inductances were individually adjustable from 0 to 15 μH to provide for pulse shape adjustment.

*Army Research Office/Battelle Columbus Laboratories Scientific Services Agreement

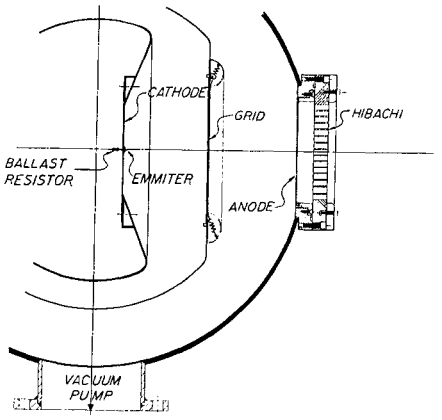

Figure 1. Triode Cross Section

A two electrode, ferrite decoupled, spark gap was used to switch the PFN. An inverse diode and an end of line clipper are not used since a spark gap is a bidirectional current conductor.

Ten parallel 9.3 m long 50 Ω cables were used to connect the PFN output to an oil insulated 17:1 step up pulse transformer. The transformer secondary is conected between the electron beam cathode and the grounded anode.

A trigger transformer is connected between the cathode and the 48 resistively isolated cathode emission sites. The trigger transformer is located in the oil tank with the pulse transformer and is isolated from ground for the full 300 kV maximum cathode operating voltage. Pulsed voltages in the range 5 to 25 kV with 0.5 μsec pulsewidth are used for cathode initiation. Less than 10 mJ of energy is required for each cathode surface flashover site.

The modulator contains a charging diode and inductor to permit operation with resonant charging up to a 50 Hz rate. A large 20 kV power supply was unavailable and the experiments reported here were performed at a repetition rate of seven seconds between pulses.

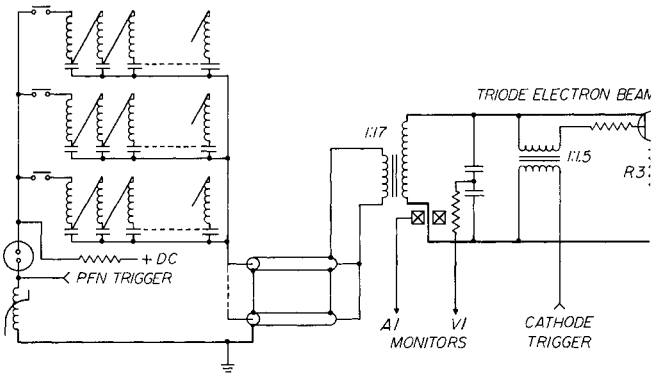

Figure 2. E-Gun Modulator Arrangement

Report Documentation Page

Form Approved
OMB No. 0704-0188

1. REPORT DATE	2. REPORT TYPE	3. DATES COVERED
JUN 1983	**N/A**	**-**

4. TITLE AND SUBTITLE	5a. CONTRACT NUMBER
Temporal Waveshaping Of A Triode Cold Cathode Electron Beam Gun	5b. GRANT NUMBER
	5c. PROGRAM ELEMENT NUMBER
6. AUTHOR(S)	5d. PROJECT NUMBER
	5e. TASK NUMBER
	5f. WORK UNIT NUMBER
7. PERFORMING ORGANIZATION NAME(S) AND ADDRESS(ES)	8. PERFORMING ORGANIZATION REPORT NUMBER
Beta Development Corporation, 6557 Sierra Lane Dublin, CA 94566	
9. SPONSORING/MONITORING AGENCY NAME(S) AND ADDRESS(ES)	10. SPONSOR/MONITOR'S ACRONYM(S)
	11. SPONSOR/MONITOR'S REPORT NUMBER(S)

12. DISTRIBUTION/AVAILABILITY STATEMENT

Approved for public release, distribution unlimited

13. SUPPLEMENTARY NOTES

See also ADM002371. 2013 IEEE Pulsed Power Conference, Digest of Technical Papers 1976-2013, and Abstracts of the 2013 IEEE International Conference on Plasma Science. Held in San Francisco, CA on 16-21 June 2013. U.S. Government or Federal Purpose Rights License.

14. ABSTRACT

15. SUBJECT TERMS

16. SECURITY CLASSIFICATION OF:			17. LIMITATION OF ABSTRACT	18. NUMBER OF PAGES	19a. NAME OF RESPONSIBLE PERSON
a. REPORT	b. ABSTRACT	c. THIS PAGE			
unclassified	**unclassified**	**unclassified**	**SAR**	**4**	

Diagnostics

The electron beam gun cathode to anode voltage was measured with a Stangenes Model CVD-200 capacitive voltage divider and the total cathode current was measured with a Pearson Model 110 pulse current transformer. The monitor locations are shown in Figure 2. The signals were routed on coaxial cables to a screen room and recorded on a Nicolet Explorer III digital oscilloscope. The data was stored on floppy discs for future analysis and computer processing.

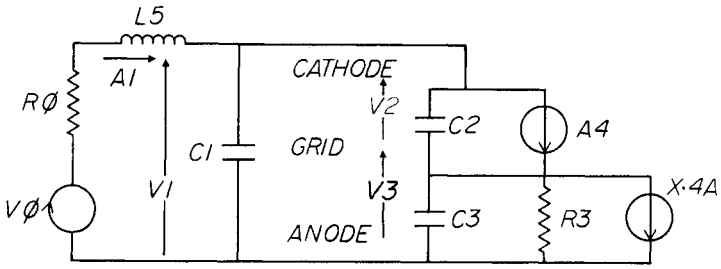

Figure 3. Triode E-Gun Model

E-Gun Model

The lumped element e-beam gun model used is shown in Figure 3. The current source A4 represents the cathode emission and is described mathematically by the Child's Law expression:

$$A4 = 2.335 \times 10\text{-}6 \; A \; V2^{3/2}/d^2(1\text{-}T/T4)^2 \qquad (1)$$

where: A is the e-beam area
V2 is the grid to cathode voltage
d is the grid-cathode separation
T is the time variable
T4 is the closure time

The closure time T4 is equal to the ratio d/V where V is the cathode plasma closure velocity. The current X · A4 in Figure 3 represents the current transmitted through the grid, where X is the fraction of the cathode current transmitted. X is about 80%. V0 and R0 represent the open circuit PFN voltage and PFN impedance, respectively, reflected to the transformer secondary. The series inductance L5 was determined by measuring the shorted transformer secondary winding current waveform and matching the risetime with a L5/R0 time constant. The capacitance values of C2 and C3 were determined from bridge measurements of the grid-anode capacitance with the cathode to anode circuit open and shorted and conversely. These values were C2 = .675 nF and C3 = .6 nF which are close to the calculated values of C2 = 0.65 nF and C3 = 0.5 nF. The calculations did not consider the bushing nor external mounting capacitance. C1 = 0.3 nF and is composed of the sum of the e-gun input capacitance and the 0.175 nF pulse transformer stray capacitance. The grid resistance, R3, was a liquid resistor whose value was adjusted by changing its copper sulfate concentration. R3 values were determined by applying a 115 V, 60 Hz source and measuring the resulting current. The closure time T4 was equated to the measured time from e-gun voltage onset to sudden voltage drop and current rise. This is illustrated in Figure 4. This sudden voltage drop did not occur on every pulse but when it occurred, the time to voltage drop was consistently between 8 and 9 μsec. The value T4 = 8 μsec is used when the calculations are compared with experiment. During initial e-gun experiments no closure was noted for pulsewidths exceeding 10 μsec.

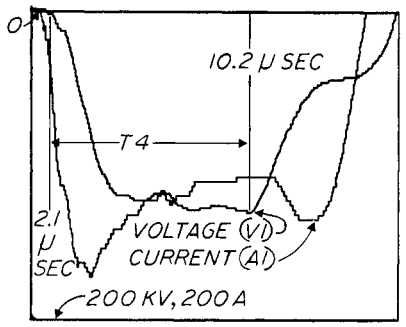

Figure 4. E-Gun Voltage and Current With Closure

The cause of the closure illustrated in Figure 4 is not understood and is being actively investigated. A program was written for the Hewlett Packard Model 85 Personal Computer to solve the equations describing the circuit shown in Figure 3. The results obtained for three sample cases agreed with the outputs of SUPER-SCEPTRE and TRACAP cirucit analysis programs.[5] The temporal behavior of the voltage V1 and current A1 was calculated for different e-gun operating conditions and compared to the corresponding experimentally measured values.

Results

Sensitivity Analysis

The circuit parameters shown in Figure 3 were varied to determine their influence on e-gun impedance and transient behavior. The components connected between the grid and anode had the greatest influence on the e-gun performance and the external components V0, R0, L5, and C1 had the least influence. For the cases investigated the e-gun impedance was approximately constant for V0 values between 200 and 600 kV. Below 200 kV the impedance rose gradually to 20% above its steady state value at V0 = 50 kV. Also, the e-gun impedance was insensitive to the beam area A of Equation 1. The e-gun impedance only decreased by about 3% when the beam area was reduced to 10% of the full aperture value. R0, L5, and C1 did not strongly effect the steady state impedance but did effect the transient behavior. The e-gun voltage rise time increased with increasing values of L5 and C1. Hence, these circuit elements should be minimized.

A sequence of figures will be used to illustrate the e-gun performance dependence on the circuit components shown in Figure 3. Unless otherwise stated the following standard conditions will be used in the figures: V0 = 400 kV, R0 = 843 ohms, L5 = 1.2 mH, C1 = 0.3 nF, C2 = 0.675 nF, C3 = 0.6 nF, X = .8, T4 = 8 μsec, A = 3,000 cm^2, d = 15 cm, and R3 = 5900 Ω. The e-gun impedance is primarily determined by the value of the grid-andode resistance R3 and the grid transmission fraction X. The e-gun impedance monotonically increases with increasing R3 values, as illustrated in Figure 5, and e-gun closure reduces the impedance from the no closure value. In Figure 5 the no closure case was calculated by letting T4 = ∞ and the impedance with closure was obtained by calculating the ratio of V1 to A1 at 6.5 μsec with T4 = 8 μsec. The impedance value at 6.5 sec is used to facilitate comparison with experiments. The difference between the two curves in Figure 5 is exaggerated at large R3 values due to rise time effects. The steady state impedance with closure is not achieved at 6.5 sec at large R3 values. The e-gun impedance decreases with increasing grid transmission. This is illustrated in Figure 6 for the four values of grid resistance R3 investigated in this work.

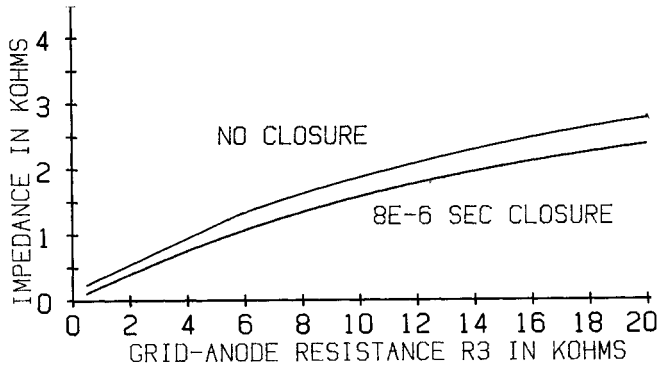

Figure 5. E-Gun Impedance vs Grid Resistance R3.

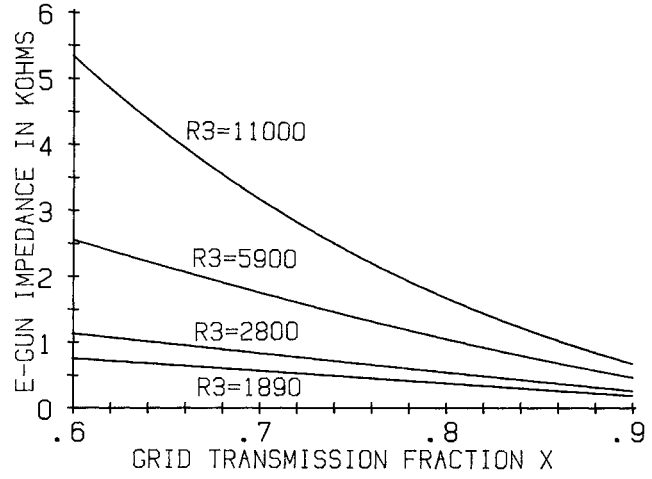

Figure 6. E-Gun Impedance vs Grid Transmission Fraction X.

The e-gun voltage rise time behavior is illustrated in Figures 7, 8, and 9. In Figure 7 it is shown that the voltage rise time increases with inreasing values of grid-anode capacitance C3 and illustrates the need to minimize this capacitance.[4] Unfortunately C3 is difficult to reduce because the major contributor to this capacitance is the value associated with the concentric grid and anode cylinders. Hence, other means must be used to reduce the e-gun voltage rise time.

The voltage rise time can be improved by adding capacitance between the grid and cathode. This is illustrated in Figure 8 where it is shown that the voltage rise time can be improved by a factor of two if 4 nF is added to the residual C2 value of 0.675 nF.

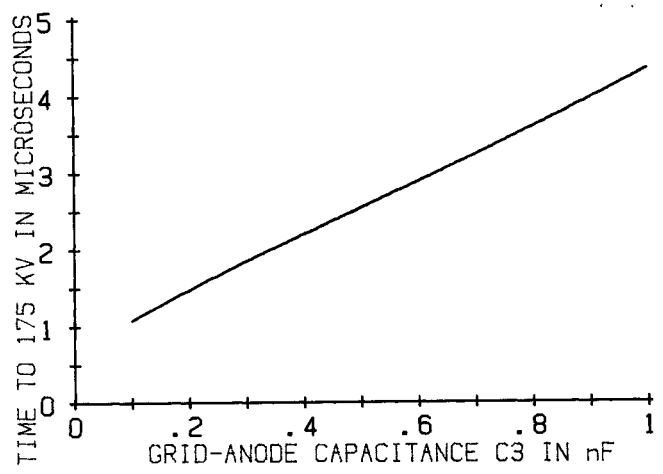

Figure 7. Voltage Rise Time vs Grid-Anode Capacitance C3.

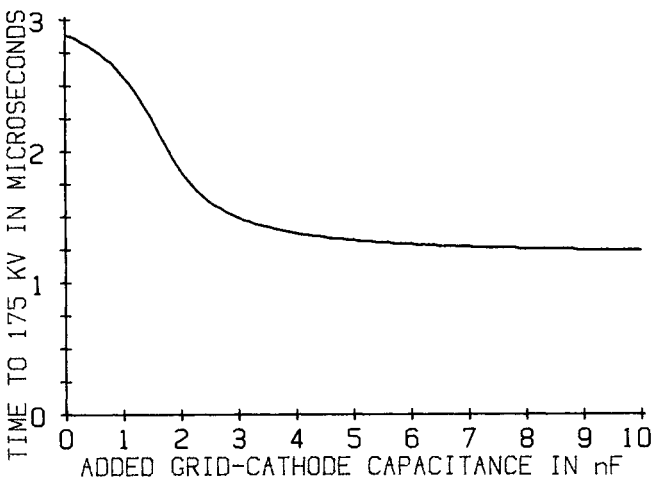

Figure 8. Voltage Rise Time vs Added Grid-Cathode Capacitance

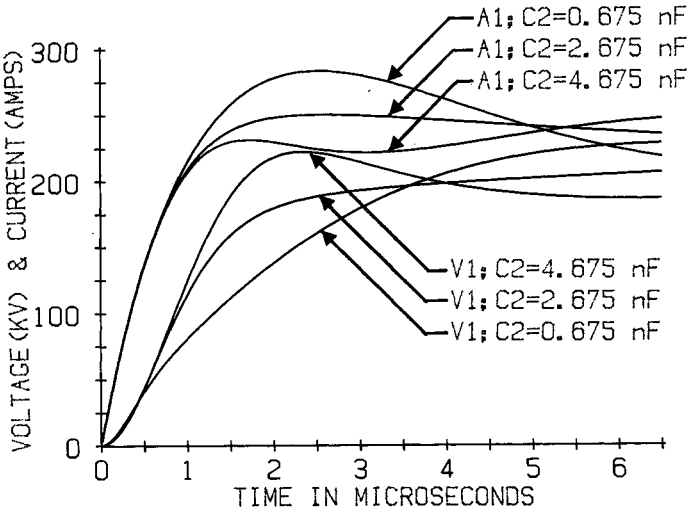

Figure 9. E-Gun Voltage and Current Variation For Different C2 Values.

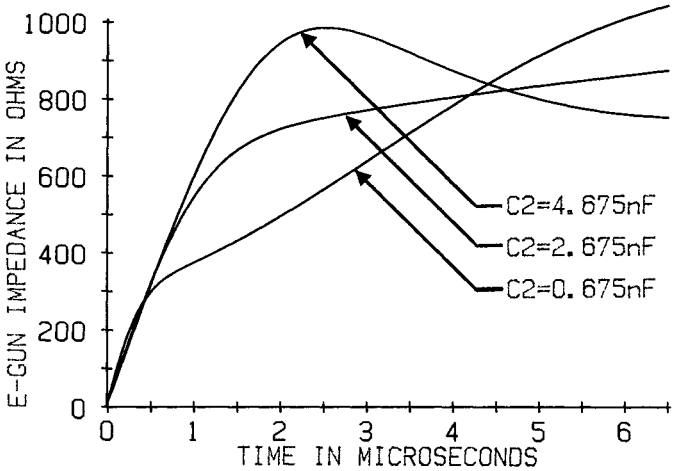

Figure 10. E-Gun Impedance Variation For Different C2 Values.

The temporal behavior of the e-gun voltage and current for different C2 values is shown in Figure 9. The voltage rise time improvement for increasing C2 values is apparent. It is seen that for C2 = 2.675 nF the voltage is fairly flat and for C2 = 4.675 nF a voltage overshoot occurs. Also illustrated in Figure 9 is the decrease of the initial current peak and the higher values of late time current occurring when C2 is increased. The

temporal variation of e-gun impedance is illustrated in Figure 10. It is seen that a moderation of the e-gun impedance variations can be accomplished with a proper choice of C2. Very flat impedance profiles were calculated for X = .7 (i.e., reduced transmission from the standard case) and C2 = 2.675 nF.

Experimental Comparison

The measured and calculated e-gun impedance values are compared in Table I for four different grid resistance values. The measured values had a ± 6% deviation from the mean values listed in the table. If the extremes of the error bounds are used reasonable agreement between theory and experiment is obtained for a grid transmission value between .78 and .79. However, if the impedances in the individual rows are matched, increasing values of grid transmission, toward the geometrical limit of .8, have to be used as R3 increases. This may be a real effect because at constant gun current the grid to cathode electric field will increase with increasing R3 values. The increased electric field could alter the electron trajectories in the cathode-grid region.

Table I. Comparison of Measured and Calculated Values of Gun Impedance, Z1, For Different Grid Transmission Fractions, X, and Grid-Anode Resistances, R3.

GRID	MEASURED	CALCULATED Z1 (Ω)			
R3 (Ω)	Z1 (Ω)	X = .8	X = .78	X = .77	X =.76
1,890	440	372	410	430	449
2,800	638	539	597	626	656
5,900	1,162	1,047	1,178	1,246	1,315
11,000	1,689	1,670	1,923	2,058	2,199

TDK, Incorporated 1 nF, 50 kV ceramic capacitors were added between the grid and anode to improve voltage rise time. The experimental and calculated temporal voltage behavior is compared in Figure 11 for C2 = 0.675 nF and C2 = 4.675 nF and the temporal variation of current is compared in Figure 12. For C2 = 0.675 nF. Good agreement is obtained between the calculated and experimental behavior.

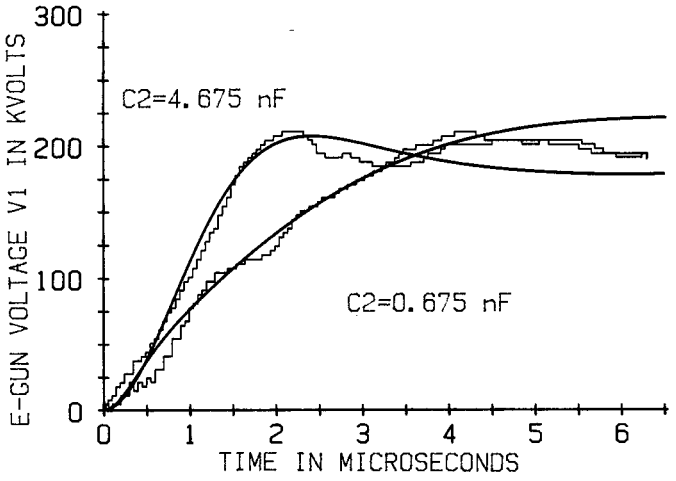

Figure 11. Comparison of Calculated and Experimental Voltage Variation.

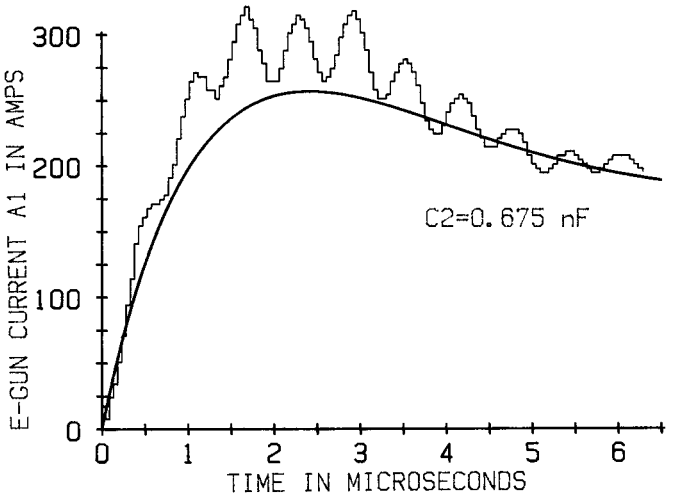

Figure 12. Comparison of Calculated and Experimental Current Variation.

Figures 11 and 12 were generated by plotting the output of the Nicolet Explorer III Digital Oscilloscope directly onto calculated curves. The grid transmission fraction X was taken to be .78 based on the data shown in Table I. The open circuit voltage V0 was adjusted in the calculations to match the experimental data. The following values were used: V0 = 370 kV for C2 = 0.675 nF and V0 = 360 kV for C2 = 4.675 nF. The charging voltage was not measured in the experiments. It was adjusted during each experimental condition investigated to produce e-gun voltages of about 200 kV. The comparison of calculated and experimental currents for C2 = 4.675 nF is not shown due to page restrictions. The experimental data agreed with the shape of the calculated curve in that a central dip and a positive end of pulse slope was measured. (See, Figure 9 for calculated shape.) However, the amplitude agreement was not as good as for the C2 = 0.675 nF case shown in Figure 12. For C2 = 4.675 nF, at 6 μsec the calculated value was about 13% lower than the experimentally measured current.

Conclusion

The model shown in Figure 3 was found to adequately describe the general behavior of a wide area triode electron beam gun. Good agreement between theory and experiment was obtained of e-gun impedance dependence on grid resistance. Also, the predicted voltage rise time improvement obtained by increasing the e-gun grid to cathode capacitance was experimentally verified. Model refinements are needed to describe the observed high frequency voltage and current variations.

References

1. G. K. Loda, Proc 2nd Int'l Topical Conf on High Power Electron and Ion Beam Research and Tech Vol II, Lab of Plasma Studies, Cornell Univ pp 879-890, Oct 3-5, 1977.
2. G. A. Mesyats et al., in 4th Int. Symp. on Discharges and Electron Insulation in Vacuum, p 82, Sep 1-4, 1970.
3. W. T. Leland, et al., LANL Report No. LA-7186, Jul 1978.
4. W. T. Leland and M. Kirchner, LANL Report No. LA-UR-82-1088.
5. R. Limpaecher, Super-Sceptre; J. R. Hall, TRACAP Comparison.